

Field-free molecular alignment detection by $4f$ coherent imaging

J. Houzet · F. Billard · E. Hertz · D. Chateau ·
F. Chaussard · B. Lavorel · O. Faucher

Received: 21 March 2012/Revised: 11 July 2012/Published online: 22 September 2012
© Springer-Verlag 2012

Abstract Time-resolved detection of field-free molecular alignment is investigated by phase contrast. The technique based on a $4f$ imager operating as an inverted Zernike spatial filter makes it possible to discriminate between positive and negative molecular alignment revivals produced in a linear molecule. The measurements are performed in a way that minimizes the contamination of the signal by the plasma generated during the aligning pulse. The observations are supported by a semi-analytical model, from which the degree of alignment produced at the beam focus is estimated.

1 Introduction

Field-free alignment, also known as nonadiabatic alignment, is a process that occurs when non-spherical molecules are exposed to a short and intense laser pulse [1]. The nonresonant interaction driven by a pulse of duration much shorter than the classical rotational period results in the production of postpulse transient molecular alignment revivals. The possibility of confining in space the rotational axes of a molecule, in the absence of strong driving field, has been found particularly useful in various fields extending to high harmonic generation and attophysics [2], molecular tomography [3], molecular-frame photoelectron angular distribution [4], laser filamentation [5], control of molecular scattering [6], and so forth.

Some of the aforementioned applications require a large number density of molecules (10^{23} – 10^{26} m $^{-3}$) that restricts the detection to optical methods. Optical probing of molecular alignment relies on the all-optical Kerr effect produced by the reorientation of the molecular dipoles leading to a change in the refractive index [7]. Depending on the detection scheme, the optical probe allows either the retrieval of $\langle \cos^2 \theta \rangle - 1/3$ or its squared value, with $\langle \cos^2 \theta \rangle$ the quantum expectation value and θ the angle between the molecular axis and the direction of the field.

The present work investigates the phase-sensitive detection of alignment revivals through time-resolved $4f$ coherent imaging [8], enabling a direct observation of $\langle \cos^2 \theta \rangle - 1/3$. It provides a simple and readily implementable technique allowing to monitor field-free revivals, as well as to discriminate between alignment ($\langle \cos^2 \theta \rangle > 1/3$) and planar delocalization ($\langle \cos^2 \theta \rangle < 1/3$). The present $4f$ coherent imager is inspired by the Zernike phase-contrast technique [9] used in microscopy. In the latter, the phase shifting filter and the unknown phase object are located at the Fourier and input plane of a $4f$ imager system, respectively. In the former, the filter is placed at the input plane of the imager in order to get information about the field-induced nonlinear phase produced at the Fourier plane of the imager, as originally proposed by Boudebs et al. [10] and recently implemented in a pump-probe version [11].

2 Experiments

The experimental setup is depicted in Fig. 1. A static cell (not represented) of CO $_2$ molecules placed at the Fourier plane of the $4f$ imager is first exposed to a linearly polarized strong pump pulse, whose large intensity is

J. Houzet · F. Billard · E. Hertz · D. Chateau · F. Chaussard ·
B. Lavorel · O. Faucher (✉)
Laboratoire Interdisciplinaire Carnot de Bourgogne (ICB),
UMR 6303 CNRS-Université de Bourgogne, BP 47870,
21078 Dijon Cedex, France
e-mail: Olivier.Faucher@u-bourgogne.fr

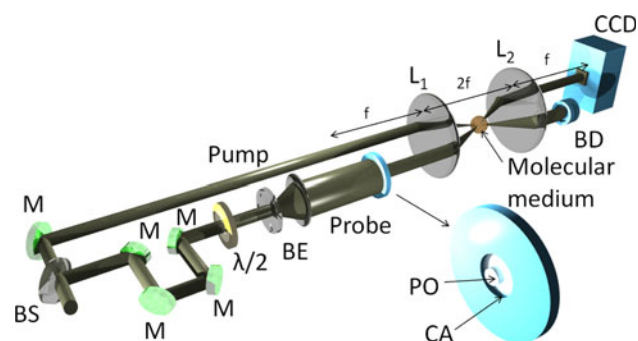


Fig. 1 Pump-probe setup of the $4f$ coherent imager. *BS* beam splitter, *M* mirrors, *BE* beam expander ($4\times$), *PO* phase object, *CA* circular aperture, *BD* beam dump, *CCD* charge-coupled device. L_1 , L_2 : $f = 200$ mm lenses

responsible for a field-free alignment of the molecules. The nonlinear time-dependent refractive index resulting from this alignment is then experienced by a time-delayed probe pulse of the same frequency. The polarization of the probe pulse can be set either parallel or perpendicular to the pump pulse, depending on the orientation of the half-wave plate. For better sensitivity, the input probe beam is filtered by a circular aperture (CA) of radius $R_a = 4.5$ mm, so that its spatial profile is almost top hat. The phase-sensitive detection is performed by inserting in the central part of the top hat beam a phase object (PO), i.e. a thin film of fused silica of radius $L_P = 1.5$ mm, inducing a $\pi/2$ phase shift at 800 nm [12]. The CA and the PO are located at the object plane of the imager. Both pulses are derived from a chirped pulse-amplified Ti:sapphire femtosecond laser. The system provides 100 fs-duration pulses at a repetition rate of 1 kHz, with a wavelength centered at 800 nm. The intensity of the second pulse is limited so that the alignment produced by the probe alone can be disregarded. The crossing angle between the two beams is $\sim 4^\circ$.

3 Results and discussion

The phase-contrast image of the probe recorded with parallel field polarizations and a pump-probe delay set to $T_R/4$, with $T_R \simeq 42.7$ ps the rotational period of CO_2 [13], is shown in Fig. 2a. The contrast between the inner disk (PO's image) and the outer ring (CA's image) is due to the accumulated nonlinear phase induced by field-free alignment along the propagation of the probe. The signal depicted in Fig. 2b is an average over 180 lineouts measured by a step of 1° . We see that the transmission change ΔT is negative, meaning that $\langle \cos^2 \theta \rangle < 1/3$ for $T_R/4$. This is consistent with the fact that the quarter revival is produced by molecules delocalized in a plane perpendicular to the field polarization. The measurement of Fig. 2 has been repeated for different values of the pump-probe delay. In

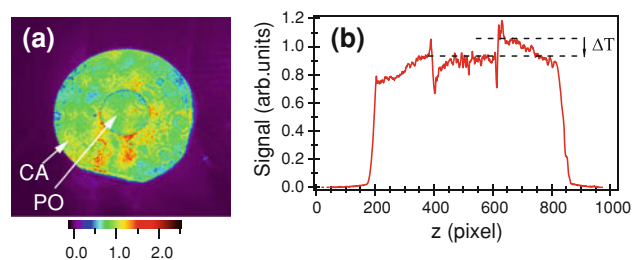


Fig. 2 **a** Phase-contrast image recorded in CO_2 by a CCD camera (exposure time of 82 ms). **b** Lineout through the image center normalized to unity. ΔT , transmission change

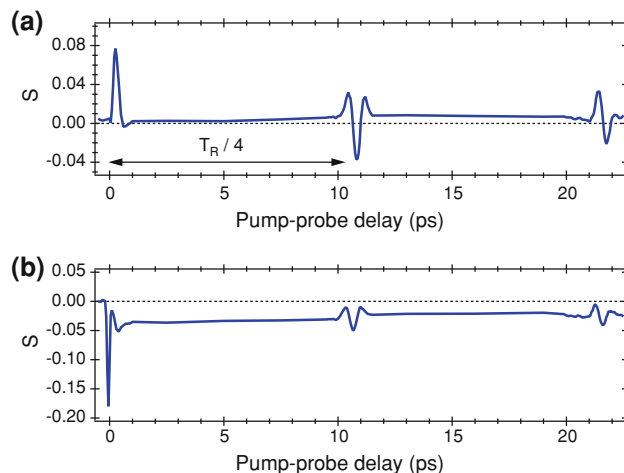


Fig. 3 Signals deduced from the phase-contrast images recorded for different delays at an averaged intensity of the aligning pulse of **a** 15 and **b** 48 TW/cm^2

order to improve the signal-to-noise ratio, the normalized transmission $S = (S_{PO} - S_{CA})/S_{CA}$ has been evaluated for each delay, with S_{PO} and S_{CA} defining the signal averaged over the image of the phase object (PO) and circular aperture (CA), respectively. The results are shown in Fig. 3 for a low (a) and high (b) intensity of the aligning laser. Each data point results from an average over 30 images similar to the one presented in Fig. 2. At low intensity, the signal displays the well-known temporal structures, featuring the field-free alignment of a homonuclear molecule, i.e. a series of revivals spaced by $T_R/4$ alternating between positive (alignment) and negative (planar delocalization) values [14]. The positive peak observed around the zero delay results from the rotational and electronic contributions to the Kerr effect. For higher intensity, the alignment signal is substantially altered by the presence of the long-living plasma resulting from ionization of the gas by the pump pulse. The negative phase introduced by the free electrons leads to a persistent negative shift of the contrast at positive delays as observed in Fig. 3b. Another intensity effect is the large negative signal observed around the zero delay as in birefringence measurements [15].

In order to support the experimental observations, we carry out a numerical model of the phase-contrast method applied to molecular alignment detection. For that purpose, we consider at the front focal plane of the first lens (L_1) a pump pulse with a Gaussian wavefront given by

$$E_P(r, t) = \mathcal{E}_P(t) \exp(-r^2/w_0^2) \exp(i\omega t), \tag{1}$$

with $\mathcal{E}_P(t)$ a slowly varying amplitude taking into account the temporal distribution, w_0 the beam radius defined at $1/e^2$ of the peak intensity, ω the angular frequency, and r the radial space coordinate. Neglecting the finite extent of the lens, the pump field at the back focal plane of the lens is given by the spatial Fourier transform of the input wavefront

$$E_P(u, t) = 2\pi \int_0^\infty E_P(r, t) J_0(2\pi r u) r dr, \tag{2}$$

where $u = r'/\lambda f$ and r' are, respectively, the radial spatial frequency and space coordinate at the Fourier plane, f is the focal length, and J_0 is the zeroth order Bessel function. The molecules exposed to the pump field undergo a field-free alignment leading to a spatial and temporal modulation of the refractive index. Along a direction parallel and perpendicular to the field, the change in the index of refraction is described by

$$\Delta n_{\parallel}(u, t) = \frac{N\Delta\alpha}{2\epsilon_0} (\langle \cos^2 \theta \rangle(u, t) - 1/3) \tag{3}$$

and

$$\Delta n_{\perp}(u, t) = -\frac{1}{2} \Delta n_{\parallel}(u, t), \tag{4}$$

respectively [13]. In these expressions, N is the number density of molecules, ϵ_0 is the vacuum permittivity, and $\Delta\alpha = \alpha_{\parallel} - \alpha_{\perp}$ is the anisotropy of polarizability, with α_{\parallel} and α_{\perp} being the polarizability components parallel and perpendicular to the molecular axis, respectively. $\langle \cos^2 \theta \rangle - 1/3$ is calculated by solving the time-dependent Schrödinger equation [13] assuming a gas sample of initial temperature $T_0 = 300$ K and an intensity of the field at the back focal plane of L_1 given by

$$I_P(u, t) = I_0(t) \exp(-2\pi^2 w_0^2 u^2), \tag{5}$$

as determined from the product $E_P(u, t) E_P(u, t)^*$ calculated by using (1) and (2), with $I_0(t)$ the temporal intensity.

As shown in Ref. [16], the spatial Fourier transform of the time-delayed probe pulse at the back focal plane of L_1 is given by

$$E_{Pr}(v, t') = [\mathcal{B}(v) + \rho^2(i-1)\mathcal{B}(v\rho)] \mathcal{E}_{Pr}(t') \exp(i\omega t'), \tag{6}$$

where $\mathcal{E}_{Pr}(t')$ is the temporal envelope of the probe pulse, $t' = t - \tau$, with τ the temporal delay between the two

pulses, $v = 2\pi u R_a$, $\rho = L_P/R_a$, $\mathcal{B}(x) = 2J_1(x)/x$ is the Besinc function with $J_1(x)$ the first-order Bessel function. The Besinc function $\mathcal{B}(v)$ (resp., $\mathcal{B}(v\rho)$), describes the probe field filtered through the circular aperture CA (resp., phase object PO) depicted in Fig. 1. In the presence of the pump field, the molecular alignment imprints on the wavefront of the probe field a nonlinear phase shift $\phi_{NL}(u, t) = (2\pi/\lambda)L\Delta n(u, t)$, reflecting the temporal dynamics induced by the pump process at time t , with L the interaction length between the two pulses and λ the wavelength. For parallel and perpendicular polarization, we have $\Delta n(u, t) = \Delta n_{\parallel}(u, t)$ and $\Delta n(u, t) = \Delta n_{\perp}(u, t)$, respectively. The probe field distribution in the back focal plane of the second lens (L_2), i.e. the image plane of the $4f$ setup, is obtained through the Fourier transform of the phase-shifted field $E_{Pr}(v, t') \exp[i\phi_{NL}(v, t)]$ resulting in

$$E_{out}(r, t, t') = \mathcal{E}_{Pr}(t') [\text{circ}(r/R_a) + (i-1)\text{circ}(r/L_P) + \alpha(r, t)], \tag{7}$$

where $\text{circ}(x)$ stands for the circle function. The two first terms on the right-hand side of this equation correspond, respectively, to the image of the circular aperture and the phase object, whereas the third term $\alpha(r, t) = a_0(r, t) + (i-1)a_1(r, t)$ represents the modification of the field image introduced by the pump-induced alignment with

$$a_j(r, t) = \int_0^\infty \{\exp[i\phi_{NL}(v_j, t)] - 1\} J_0(v_j r/R_a) J_1(v) dv, \tag{8}$$

$j = 0, 1$, $v_0 = v$, and $v_1 = v/\rho$ [16]. Finally, from the intensity integrated over the time response of the CCD camera pixels

$$I_{out}(r, \tau) \propto \int_{-\infty}^\infty |E_{out}(r, t, t')|^2 dt', \tag{9}$$

we define

$$S_{PO}(\tau) = \frac{\int_0^{L_P} 2\pi r I_{out}(r, \tau) dr}{\int_0^{L_P} 2\pi r dr} \tag{10}$$

and

$$S_{CA}(\tau) = \frac{\int_{L_P}^{R_a} 2\pi r I_{out}(r, \tau) dr}{\int_{L_P}^{R_a} 2\pi r dr}, \tag{11}$$

the signal integrated over the image of the phase object and circular aperture, respectively.

The expectation value $\langle \cos^2 \theta \rangle - 1/3$ has been calculated for CO_2 at different intensities up to 100 TW/cm^2 . The maximum value produced at $3T_R/4$ is shown in Fig. 4a. The corresponding value of the nonlinear phase ϕ_{NL} estimated from the experimental conditions, i.e. $P = 1$

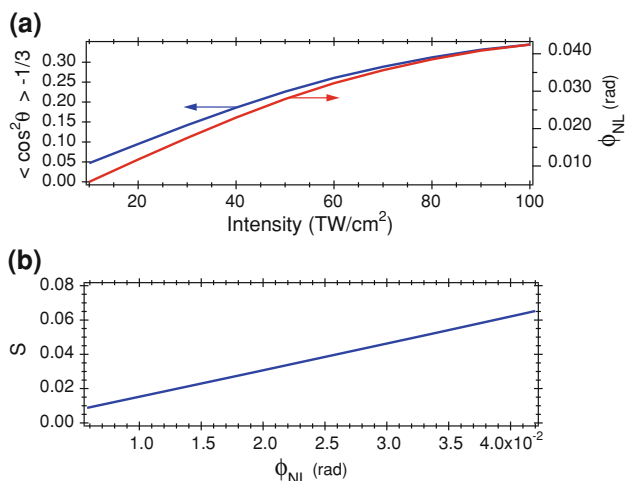


Fig. 4 **a** $\langle \cos^2 \theta \rangle - 1/3$ (left-hand scale) and the corresponding nonlinear phase (right-hand scale) versus intensity calculated in CO₂ at $3T_R/4$, at room temperature, and for a pulse duration of 100 fs. **b** Normalized transmission change S versus nonlinear phase

bar, $T = 300$ K, $\rho = 0.34$, and $L = 0.05$ mm, is shown on the right-hand scale. Figure 4b displays the value of the normalized transmission change S deduced from the calculation of (10) and (11) for the same intensities as in Fig. 4a. In order to account for optical aberrations and imperfections of the laser beam profile, the calculations have been performed with a focal length f set to 240 mm (instead of 200 mm) so as to obtain a probe beam radius that matches the one measured at the Fourier plane of L_1 , i.e. 22 μm . The results show that the relation between S and ϕ_{NL} is linear, in agreement with the theory that predicts a linear detection for $\phi_{NL} < \phi_{\text{max}}$, where $\phi_{\text{max}} \simeq 4.2$ rad for $\rho \simeq 0.34$ [16].

A comprehensive analysis of the experimental data presented in Fig. 3 would require the plasma to be included in the model. Compared to alignment, the plasma generation by a 800 nm pulse is a much higher-order process with respect to intensity. Introducing the plasma effect in the simulations would therefore lead to an estimation of the alignment that would be conditioned by the accuracy of the theoretical model used to describe the ionization process. The alternative proposed in this work is to remove the plasma contribution from the data by measuring the signal for two different polarizations of the probe. We have shown in Fig. 4b that the phase-contrast signal is proportional to the nonlinear phase induced by the pump. When the two pulses are polarized along the same axis, the phase experienced by the probe pulse is proportional to the alignment-induced refractive index Δn_{\parallel} . Additionally, the probe undergoes the refractive index Δn_e of the free electrons resulting from the pump ionization. The signal is therefore the sum of these two contributions: $S_{\parallel} \propto \Delta n_{\parallel} +$

$f(\Delta n_e)$, with $f()$ the function that describes the effect of the free electrons on the phase-contrast signal and Δn_{\parallel} given by (3). When the two pulses are crossed-polarized, the phase-contrast signal is $S_{\perp} \propto \Delta n_{\perp} + f(\Delta n_e)$, with Δn_{\perp} given by (4). The plasma being isotropic with respect to the polarization of the probe, its contribution to the signal is the same in both field configurations [17]. The anisotropy induced by the molecular alignment can hence be used to isolate the plasma contribution from the signal. Our method therefore consists in recording the pump-probe phase-contrast signal for each polarization, keeping all other parameters identical. Then by combining the records so that $\Delta S = 2/3(S_{\parallel} - S_{\perp}) \propto \Delta n_{\parallel}$ and $\Sigma S = 1/3(S_{\parallel} + 2S_{\perp}) \propto \Delta n_e$, one can separate the alignment and plasma contribution, respectively.

The method is tested with CO₂ exposed to two different laser intensities. The results are shown in Fig. 5. As an attempt to maintain a good signal-to-noise ratio, we shortened the acquisition time by limiting the delay range to the two first revivals. The measurements have been performed under a static pressure of 1 bar. Compared to Fig. 3, the elimination of the plasma contribution in Fig. 5a, b allows uncovering the permanent alignment effect, revealed by a positive offset in the pump-probe trace at positive delays [18]. The alignment revivals are also subject to a decay of time constant $T_{\text{coll}} \approx 60$ ps/bar due to collisions perceptible at both intensities. The alignment-free signals shown in Fig. 5c, d feature a clear decay corresponding to the lifetime of the plasma. Since the alignment of the molecules and especially their ionization are favored by the intensity, both permanent alignment and plasma decay are more noticeable at the largest intensity.

The numerical model described in this section has been used to calculate the plasma-free signal of Fig. 5a, b based

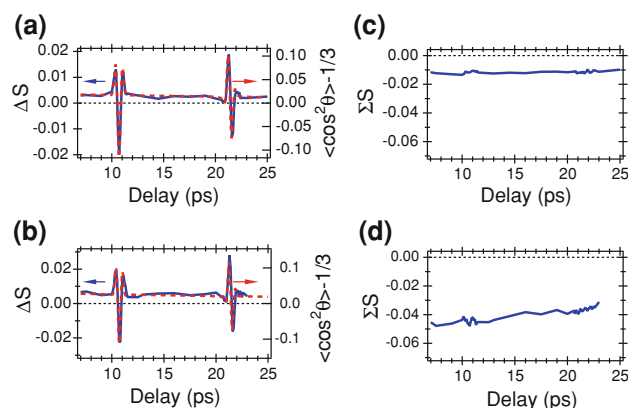


Fig. 5 Plasma-free (**a**, **b**) and molecular-free (**c**, **d**) phase-contrast signals (full blue lines, left-hand scale) recorded for an averaged intensity of 38 ± 7 TW/cm² (**a**, **c**) and 55 ± 10 TW/cm² (**b**, **d**). $\langle \cos^2 \theta \rangle - 1/3$ (red dashed lines, right-hand scale) calculated at an intensity of 38 (**a**) and 55 TW/cm² (**b**), respectively

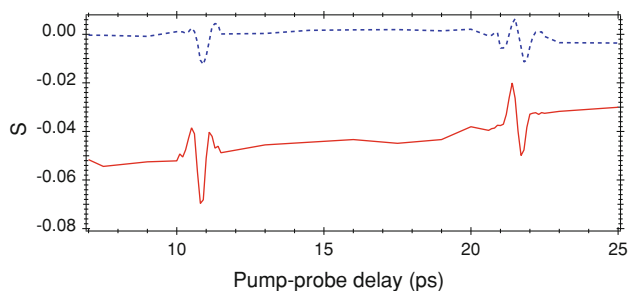


Fig. 6 Phase-contrast signals recorded with Fourier-transformed limited pulses of 100 fs duration (*full red line*) and chirped pulses of 220 fs duration (*blue dashed line*) of the same energy 110 μJ

on (10) and (11). The spatial beam profiles have been indirectly taken into account through the use of an effective intensity. As shown in a previous work [19], a reasonable match between theory and experiment can be obtained by performing the calculations at the averaged intensity estimated from the measurements of the input pulse parameters. The simulations of $\langle \cos^2 \theta \rangle - 1/3$ are shown on the right-hand scale of Fig. 5a, b.

The ability of the method to detect simultaneously alignment and plasma opens the way for an active control between these two processes. The present technique could be advantageously combined with pulse shaping strategies in order to control the ratio between alignment and plasma production. This parameter plays a dominant role in filamentation [20]. As an example, the influence of a quadratic chirp on the input pulses is depicted in Fig. 6. As shown, such a simple tailoring allows a large reduction of the plasma contribution compared to the alignment. The resulting modifications of the alignment in width and amplitude could be alleviated by using more complex pulse shapes designed by a self-learning evolutionary algorithm that would also extend the control performance.

4 Conclusions

Laser-induced field-free molecular alignment has been investigated at room temperature in CO_2 by a time-resolved phase-contrast technique. The parameters of the experiment have been introduced in a semi-analytical model for evaluating the dependence of the signal on the nonlinear phase induced by the molecular alignment. Under the present conditions, i.e. moderate gas pressure, short interaction length, and moderate temperature, the phase-contrast signal displays a linear response with $\langle \cos^2 \theta \rangle$ (θ being the angle between the molecular axis and the field) enabling therefore a quantitative evaluation of the alignment produced at the laser focus. A method to

circumvent the detrimental effect of the plasma on the measurements has also been proposed and tested for different laser intensities. For the sake of simplicity, the technique has been tested with a linear molecule. However, as with other optical-based techniques [13, 21, 22], the extending Zernike phase-contrast technique provides a measure of alignment generally involving different molecular axes. Therefore, it could be easily applied to more complex gas-phase systems including nonlinear molecules exposed to linear [23] and elliptic field excitations [24] or molecules in contact with dissipative environments [25].

As a *heterodyne* technique, the phase contrast provides a good alternative to other all-optical *homodyne* detection techniques not sensitive to the phase of the signal field like cross-defocusing [21] or degenerate four-wave mixing [22]. Furthermore, as a technique operating on a single shot basis, it does not necessarily require a combination of different measurements like in transient birefringence detection [13]. These two features, i.e. heterodyne and plasma-sensitive detections, make the present phase-contrast technique particularly relevant to improved quantitative determinations of ionization probability using the alignment signal as a calibration tool [17, 26]. It is also well suited to comparative studies of nonlinear refractive index and plasma effects occurring in the nonlinear propagation of intense laser pulses, as for instance in laser filamentation or optical pulse compression.

Acknowledgments We are grateful to J. M. Arocas for the fabrication of the phase object. This work was supported by the Conseil Régional de Bourgogne, the ANR *COMOC*, and the *FASTQUAST* ITN Program of the 7th FP.

References

1. H. Stapelfeldt, T. Seideman, *Rev. Mod. Phys.* **75**, 543 (2003)
2. S. Haessler, J. Caillat, W. Boutu, C. Giovanetti-Teixeira, T. Ruchon, T. Auguste, Z. Diveki, P. Breger, A. Maquet, B. Carré, R. Taïeb, P. Salieres, *Nat. Phys.* **6**, 200 (2010)
3. J. Itatani, J. Levesque, D. Zeidler, D. Niikura, H. Pépin, J.C. Kieffer, P.B. Corkum, D.M. Villeneuve, *Nature* **432**, 867 (2004)
4. J.L. Hansen, H. Stapelfeldt, D. Dimitrovski, M. Abu-samha, C.P.J. Martiny, L.B. Madsen, *Phys. Rev. Lett.* **106**, 073001 (2011)
5. F. Calegari, C. Vozzi, S. Stagira, *Phys. Rev. A* **79**, 023827 (2009)
6. E. Gershnel, I.S. Averbukh, *Phys. Rev. A* **82**, 033401 (2010)
7. O. Faucher, B. Lavorel, E. Hertz, F. Chaussard, in *Progress in Ultrafast Intense Laser Science*, vol. VII, vol. 100 of Springer Series in Chemical Physics (Springer, 2011), pp. 79–108
8. G. Shi, Y.B. Li, J.Y. Yang, Y.X. Wang, Y.L. Song, C.H. Wang, *J. Opt. Soc. Am. B* **26**, 420 (2009)
9. F. Zernike, *Science* **11**:345 (1955)
10. S. Cherukulappurath, G. Boudebs, A. Monteil, *J. Opt. Soc. Am. B* **21**, 273 (2004)
11. Y.B. Li, G.F. Pan, K. Yang, X.R. Zhang, Y.X. Wang, T.H. Wei, Y.L. Song, *Opt. Express* **16**, 6251 (2008)

12. G. Boudebs, S. Cherukulappurath, *Phys. Rev. A* **69**, 053813 (2004)
13. M.Z. Hoque, M. Lapert, E. Hertz, F. Billard, D. Sugny, B. Lavorel, O. Faucher, *Phys. Rev. A* **84**, 013409 (2011)
14. T. Seideman, *J.Chem. Phys.* **115**, 5965 (2001)
15. V. Lorient, E. Hertz, O. Faucher, B. Lavorel, *Opt. Express* **17**, 13429 (2009)
16. J.L. Godet, H. Derbal, S. Cherukulappurath, G. Boudebs, *Eur. Phys. J. D* **39**, 307 (2006)
17. V. Lorient, E. Hertz, B. Lavorel, O. Faucher, *J. Phys. B* **41**, 015604 (2008)
18. V. Lorient, P. Tzallas, E.P. Benis, E. Hertz, B. Lavorel, D. Charalambidis, O. Faucher *J. Phys. B* **40**, 2503 (2007)
19. A. Rouzée, V. Renard, B. Lavorel, O. Faucher, *J. Phys. B* **38**, 2329 (2005)
20. H. Cai, J. Wu, Y. Peng, H. Zeng, *Opt. Express* **17**, 5822 (2009)
21. V. Renard, O. Faucher, B. Lavorel, *Opt. Lett.* **30**, 70 (2005)
22. A. Rouzée, V. Renard, S. Guérin, O. Faucher, B. Lavorel, *Phys. Rev. A* **75**, 013419 (2007)
23. A. Rouzée, S. Guérin, V. Boudon, B. Lavorel, O. Faucher, *Phys. Rev. A* **73**, 033418 (2006)
24. A. Rouzée, S. Guérin, O. Faucher, B. Lavorel, *Phys. Rev. A* **77**, 043412 (2008)
25. T. Vieillard, F. Chaussard, D. Sugny, B. Lavorel, O. Faucher, *J. Raman Spectrosc.* **39**, 694 (2008)
26. V. Lorient, E. Hertz, B. Lavorel, O. Faucher, *Europhys. News* **39**, 18 (2008)